ANNALS OF GEOPHYSICS, 68, 1, V102, 2025; doi:10.4401/ag-9174
OPEN ACCESS

New developments in the estimation of tephra fallout hazard at Mt. Etna, in Italy, during the PANACEA project

Simona Scollo[*,1], Costanza Bonadonna[2], Alexander Garcia[3], Luigi Mereu[3,4], Michele Prestifilippo[3], Francesco Romeo[1,4,5], Laura Sandri[3], Manuel Stocchi[6]

(1) Istituto Nazionale di Geofisica e Vulcanologia, Osservatorio Etneo, Catania, Italy
(2) University of Geneva, Department of Earth Sciences, Geneva, Switzerland
(3) Istituto Nazionale di Geofisica e Vulcanologia, Sezione di Bologna, Bologna, Italy
(4) Center of Excellence CETEMPS, L'Aquila, Italy
(5) Sapienza University of Rome, Department of Information Engineering, Electronics and Telecommunications, Rome, Italy
(6) University of Bari "Aldo Moro", Department of Earth and Geoenvironmental Sciences, Bari, Italy

Article History: received September 30, 2024; acceped February 21, 2025

Abstract

Mount Etna, in Italy, is one the most active volcanoes in the world. Over the past two decades, its explosive activity has intensified, producing high eruptive columns that rise up to about 15 km above sea level. The particles ejected during these eruptions have caused numerous challenges for the population living on the volcano's slope, mainly due to difficulties in removing the deposits, but also in terms of health risks and mobility disruptions. The increase in Etna's explosive activity has led in continuous improvements in the monitoring and forecasting system adopted by the Istituto Nazionale di Geofisica e Vulcanologia, Osservatorio Etneo, since 2009, using new sensors and enhanced data collection and analysis. In this paper, we present a review of several activities carried out in the frame of the Work Package 2 (WP2) of the 'Probabilistic AssessmeNt of volCano-related multi-hazard and multi-risk at Mount EtnA (PANACEA)' project. While the PANACEA project aims at using accurate physics-based models and advanced probabilistic approaches to assess volcanic multi-hazards and identify at-risk zones, the WP2 objective is to improve previous studies on the tephra fallout hazards for Etna. In this context, various activities have been conducted such as: enrich the data collection of eruption source parameters by analysing previous studies and developing new methods for their quantification; improve hazard estimates using multi-model approaches; quantify the uncertainty in eruption source parameters. Additionally, progresses have been made in developing hazard maps that include ballistic impact analysis. These approaches may be extended to other active volcanoes where advanced monitoring and surveillance systems are in place.

Keywords: Etna volcano; Lava Fountains; Remote Sensing Observations; Numerical Modelling; Tephra Hazard Maps

1. Introduction

During explosive eruptions, tephra (volcanic ash, lapilli, bombs, and blocks) is blasted from volcanoes and represents one of the main volcanic hazards. Tephra fallout can cause building collapses, damage crops and disrupt transportation networks (Sparks et al., 1997; Wilson et al., 2012). Fine ash can also pose health risks, leading to conditions such as silicosis and chronic pulmonary diseases (Horwell and Baxter, 2006). Additionally, fine ash is extremely dangerous for aviation safety (Guffanti et al., 2005) as it can cause severe damages to aircraft engines due to the accumulation of melted glass particles and the erosion of turbine blades. It can also interfere with electronic equipment, obscure windscreens and block landing lights (Miller and Casadevall, 2000; Wilson et al., 2017; Hayes et al., 2021; Jenkins et al., 2024). Therefore, during eruptions, volcano observatories issue messages known as Volcano Observatory Notices for Aviation (VONA) to inform dispatchers, pilots, and air-traffic controllers about volcanic unrest and eruptive activity that could generate ash-cloud hazards. These messages are sent to Volcanic Ash Advisory Centers (VAACs) which, following the ICAO directives, are responsible for mitigating volcanic ash risks to aviation (Lechner et al., 2017; Barsotti et al., 2024).

Mount Etna (Catania, Italy) is one of the most active volcanoes in the world. In the past two decades, most of its activity has been explosive, with the formation of high eruption columns (reaching up to 15 km above sea level) and of extensive tephra fallout on volcano flanks. This has led the mayors of the main affected towns to implement measures such as banning the circulation of two-wheeled vehicles and reducing speed limits to 30 km/h. Hazard assessment has been widely studied, including the impact on infrastructures, transportation systems (Scollo et al., 2013) and health concerns (Barsotti et al., 2013). In 2009, the Istituto Nazionale di Geofisica e Vulcanologia, Osservatorio Etneo (INGV-OE) developed a system to support the 24/7 monitoring and surveillance activities (Scollo et al., 2009). This system combines modelling and volcanological data to estimate the main regions likely to be affected by tephra fallout and ash dispersion in the atmosphere. The modelling relies on the TEPHRA2 model (Bonadonna et al., 2005) which simulates the transport of volcanic ash and lapilli from the crater to the ground. The model requires input parameters to update the a priori information, such as the height of the eruptive column (CH), the total mass (TM) and total grain size distribution (TGSD) of the volcanic particles (Scollo et al., 2008). Wind intensity and direction are obtained from weather forecasting models (Scollo et al., 2009) received from the hydrometeorological service of ARPA in Emilia Romagna (ARPASIM). The received data is in GRIBv1 format with 12 barometric levels and a grid using Data Representation in Rotated latitude/longitude mode (TPH0: 43.000°, TLM0D: 10.000°). The grid is uniform in both directions with a 5 km resolution, and the region is defined by the following ranges: latitude (−9.000°, −1.575° and longitude (0.855°, 7.155°).

The system operates with predefined eruptive scenarios based on previous field studies. In fact, eruption source parameters (ESP) were obtained by analysis of field data (the a priori information). Specifically, the INGV-OE considers two scenarios: Strong Plume and Weak Plume. The “Strong Plume Scenario” (SPS) assumes a well-fed and powerful volcanic column reaching up to 11 km above sea level (“Strong Plume Scenario”, SPS) while the “Weak Plume Scenario” (WPS) refers to a smaller event, with a column of up to 6 km. Further details of the ESP used in the system can be found in Table 1.

Eruptive scenarios	Eruption Time	Mass eruption rate (kg/s)	Column height	Grain-size	Sigma
SPS	5 minutes	10^6	11	−0.5	1.5
WPS	3 hours	10^5	6	0.5	1.5

Table 1. Input parameters of Strong Plume Scenario and Weak Plume Scenario used at INGV-OE.

The results of these simulations are automatically transmitted to the Italian Civil Protection Department (DPC). Figures 1a and 1b illustrate the tephra fallout maps generated for the WPS and SPS, respectively. These simulations were visible in the 7/24 INGV-OE surveillance room and were sent to the Italian Civil Protection

on 16 February 2021, during the explosive event. In 2019, the volcanic ash monitoring and forecasting system was enhanced (Scollo et al., 2019), to provide greater support for volcanologists involved in the continuous surveillance service. This upgrade also included maps of the area that will be affected by the impact of larger clasts (greater than 5 cm) using the 1-D plume model of Rossi et al. (2019) that considered Gaussian profiles of velocity within the plume. When the velocity of volcanic particles is greater than the vertical velocity of the plume's cross section, they are released and their trajectories through the atmosphere are calculated until they reach the ground. Particle sedimentation is numerically derived from the equation of motion, which incorporates the effects of wind advection, drag, and gravitational forces. The model was calibrated using field data collected during 23 November 2013 (Osman et al., 2019). The fallout of these fragments affects proximal areas, extending up to about 10 km from the vent, which are easily accessible to tourists. This can lead to damage to car windshields and pose risks of injury to people, hikers and guides (Osman et al., 2019). Figures 1c and 1d show the simulation results, available to the volcanologist on duty, obtained during the paroxysmal event of Etna on 16 February 2021.

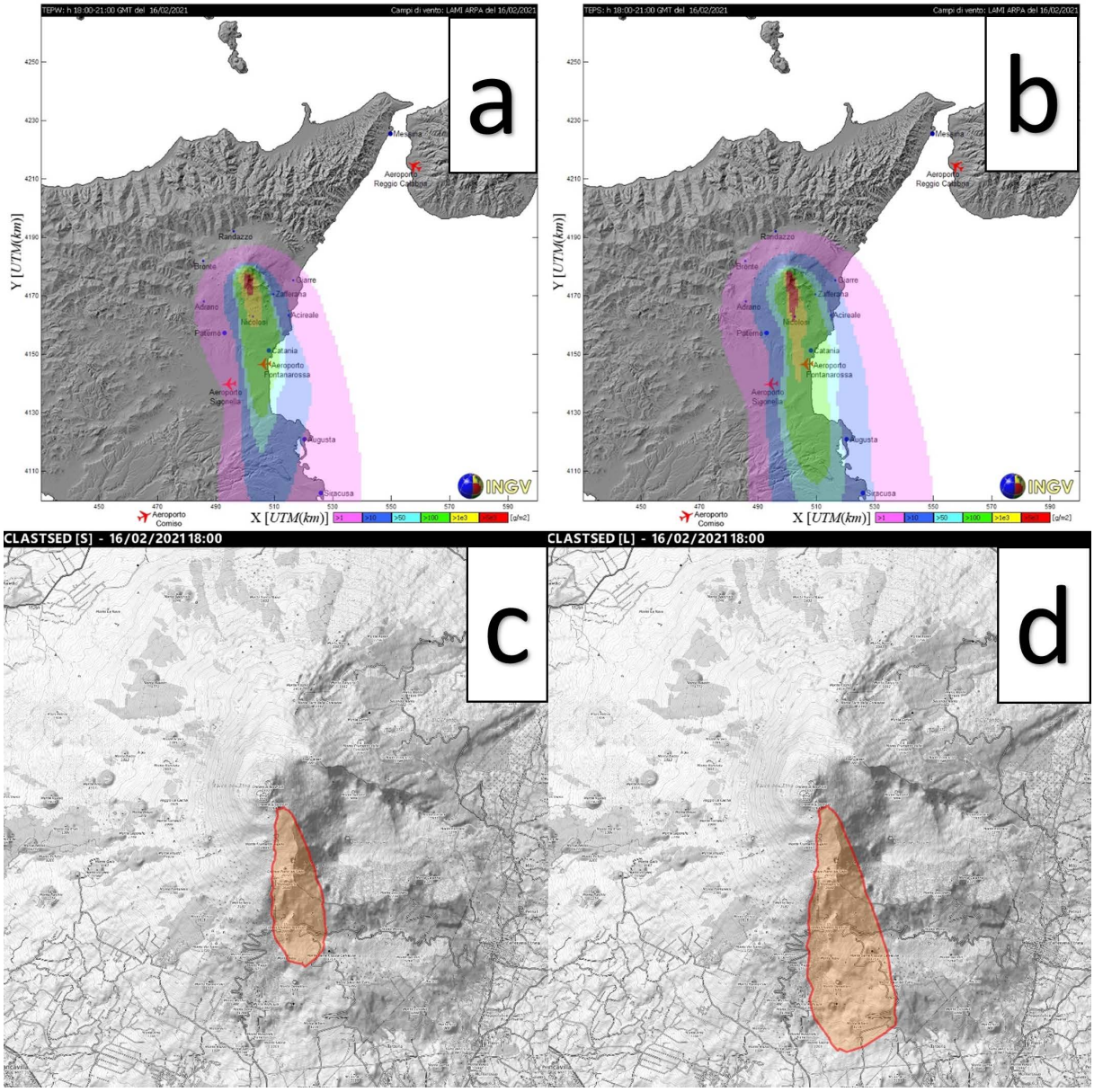

Figure 1. Examples of simulations performed using predefined eruptive scenarios: TEPHRA2 simulations run on 16 February 2021 for (a) Weak Plume scenario and (b) Strong Plume scenario (see Table 1); simulations of the area covered by larger clasts of 16 February 2021 considering an eruptive scenario similar to (c) the eruption of 12 January 2011, and (d) the eruption of 23 November 2013.

The system is continuously being improved, with updated observations from various remote sensing sources to produce more reliable simulations (Scollo et al., 2019).

In this paper, we present a review of the activities conducted within the Work Package 2 (WP2) of the 'Probabilistic Assessment of volCano-related multi-hazard and multi-risk at Mount EtnA (PANACEA)' project002E The primary objective of WP2 is to enhance previous studies on the hazards associated with tephra fallout from Etna. The WP2 includes three main tasks: (i) the 'Retrieval of eruption source parameters (ESP) for the model'. The main ESPs have been deeply analysed in order to increase the number of considered eruptive scenarios (Scollo et al., 2013); (ii) the 'Modelling and Simulation' aimed at simulating the tephra fallout deposit, and (iii) the 'Hazard Mapping'. This paper is structured as follows: Section 2 summarises the Etna explosive activity, in Section 3 we explain the methods used, Section 4 presents the main findings and results of this working group. Finally, in Section 5 we summarise the final discussions and assess future developments.

2. Explosive activity at Mt. Etna

Etna is characterised by frequent explosive activity, primarily of mild intensity. The Volcanic Explosivity Index (VEI), which is a semi-quantification of the eruption intensity (Newhall and Self, 1982), typically ranges between 2 and 3. The explosive activity observed over the last two decades is mainly characterised by the formation of lava fountains, which have been extensively documented in the literature (Andronico et al., 2021). This activity involves the summit craters and in general evolves from mild Strombolian activity to a marked increase of the explosive activity, following well-defined patterns (e.g. Alparone et al., 2003; Bonaccorso and Calvari, 2013; Calvari et al., 2018; Pioli et al., 2008; Behncke et al., 2014; Viccaro et al., 2019). During the climax, named paroxysmal phase lava fountains form high eruption columns and volcanic ash plumes that can drift hundreds of kilometers from the summit craters (Scollo et al., 2009; Calvari et al., 2011). The duration and intensity of those events can be very variable and at present, current monitoring and surveillance systems are unable to predict whether the activity will be predominantly effusive or explosive (Bonaccorso et al., 2014). Over the past twenty years, paroxysmal activity has dispersed substantial amounts of pyroclastic material with a total erupted mass up to approximately 1010 kg (Scollo et al., 2013, 2019). Flank eruptions can occur at intervals of several years, and typically produce low intensity activity that can last from a few days to months. These eruptions have the potential to cause persistent tephra fallout, primarily affecting the southeast sector of the volcano (Scollo et al., 2013). Additionally, flank eruptions can also produce extensive lava flow fields (Branca and Del Carlo, 2005). Well-studied flank eruptions occurred in 2001 and during the 2002-2003 period (Scollo et al., 2007; Andronico et al., 2008). In these events, volatile-rich, fast-rising magma erupted bypassing the central conduits, a typical behaviour for Etnean eruptions (Neri et al., 2005). During the 2001 eruption, phreatomagmatic and magmatic explosions were observed at the 2570 m-high vent, with a weak volcanic plume rising to about 5 km above sea level (a.s.l.), resulting in a southeast deposition on volcano's flanks (Scollo et al., 2007). In 2002, Etna was responsible for over 50 days of continuous tephra fallout, reaching a maximum column height of 7 km a.s.l. from a vent opened at 2750 m of altitude (Andronico et al., 2008). Figure 2 shows images of the volcanic plumes generated during the paroxysmal activity on 4 and 12 March 2021, and during the flank eruptions on 24 July 2001 and 2 November 2002.

3. Methods

3.1 Remote sensing sensors

Figure 3 provides an overview of remote sensing sensors utilised in this project. We combine data from various sensors, including ground-based cameras, radars, and satellites. The visible cameras used are VIVOTEK IP8172P, located in Catania (Etna CUAD Visible High definition camera (ECV)) and Bronte (BT). These cameras are calibrated to estimate the column height (CH) in function of the wind direction. The volcanic plume is assumed to have a negligible depth and confined to a vertical plane aligned with the wind direction. The uncertainty in the column height estimate is set $\pm$500 m (Scollo et al., 2014). We also use a thermal-infrared camera (TIR) located in Nicolosi, approximately at ~15 km from the summit crater, which can identify the height of the Incandescent Jet Region (IJR) (Mereu et al., 2020) and estimate the exit velocity of pyroclastic material. We compute the mass

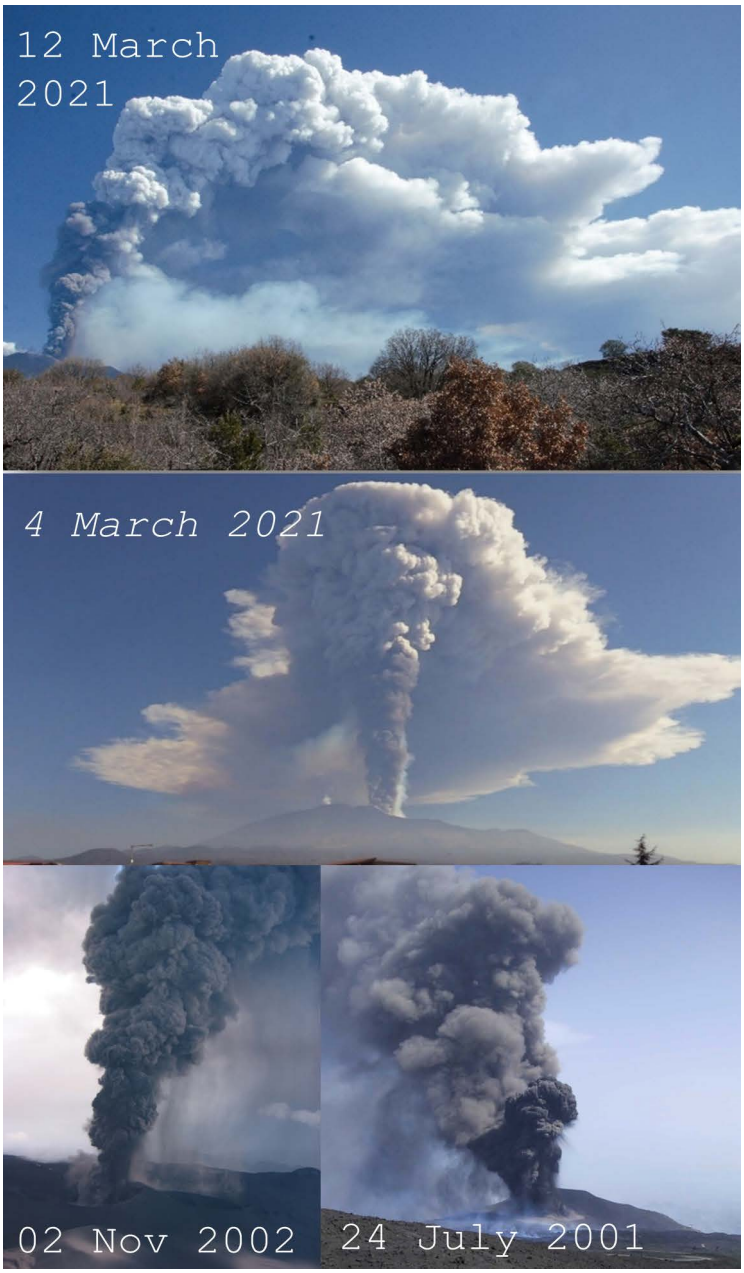

Figure 2. Eruption columns produced on: 12 March 2021. Eruption column height of 7.9 km above volcano vent (a.v.v.) (photo by Scollo S.); 4 March 2021, Eruption column height of 8.3 km a.v.v. (photo by Scollo S.); 24 July 2021. Eruption column height of 2.5 km a.v.v. (data and photo reported in Scollo et al., 2007); 2 November 2002. Eruption column height of 3.2 km a.v.v. (data and photo reported in Andronico et al., 2008).

eruption rate (MER) by knowing the size of the volcanic vent, the exit velocity and the density of the volcanic jet (Calvari et al., 2019). When CH data from the visible camera is unavailable, we estimate it by analysing satellite data. CH is derived by comparing the brightness temperature of the darkest pixel with the atmospheric temperature profile extracted from the weather forecasting model. The error in this estimate is influenced by a brightness temperature uncertainty of ± 2 K, which for Etna is less than 10% in height. Additionally, when available, we estimated the CH also using two X band weather radars, located nearby the International Airport Vincenzo Bellini (Catania) and Reggio Calabria (Reggio Calabria), and one C band radar in Monte Lauro (Siracusa) (Mereu and Scollo, 2024). The CH from these radars is estimated using the Volcanic Ash Radar Retrieval (VARR) algorithm (Marzano et al., 2012; Mereu et al., 2015). The VARR algorithm can also be used to estimate the MER and TM. Furthermore, we estimate the mass and the particle's radius of the finest particles (<10 μm radius) in the atmosphere using the radiative transfer model described in Romeo et al. (2023).

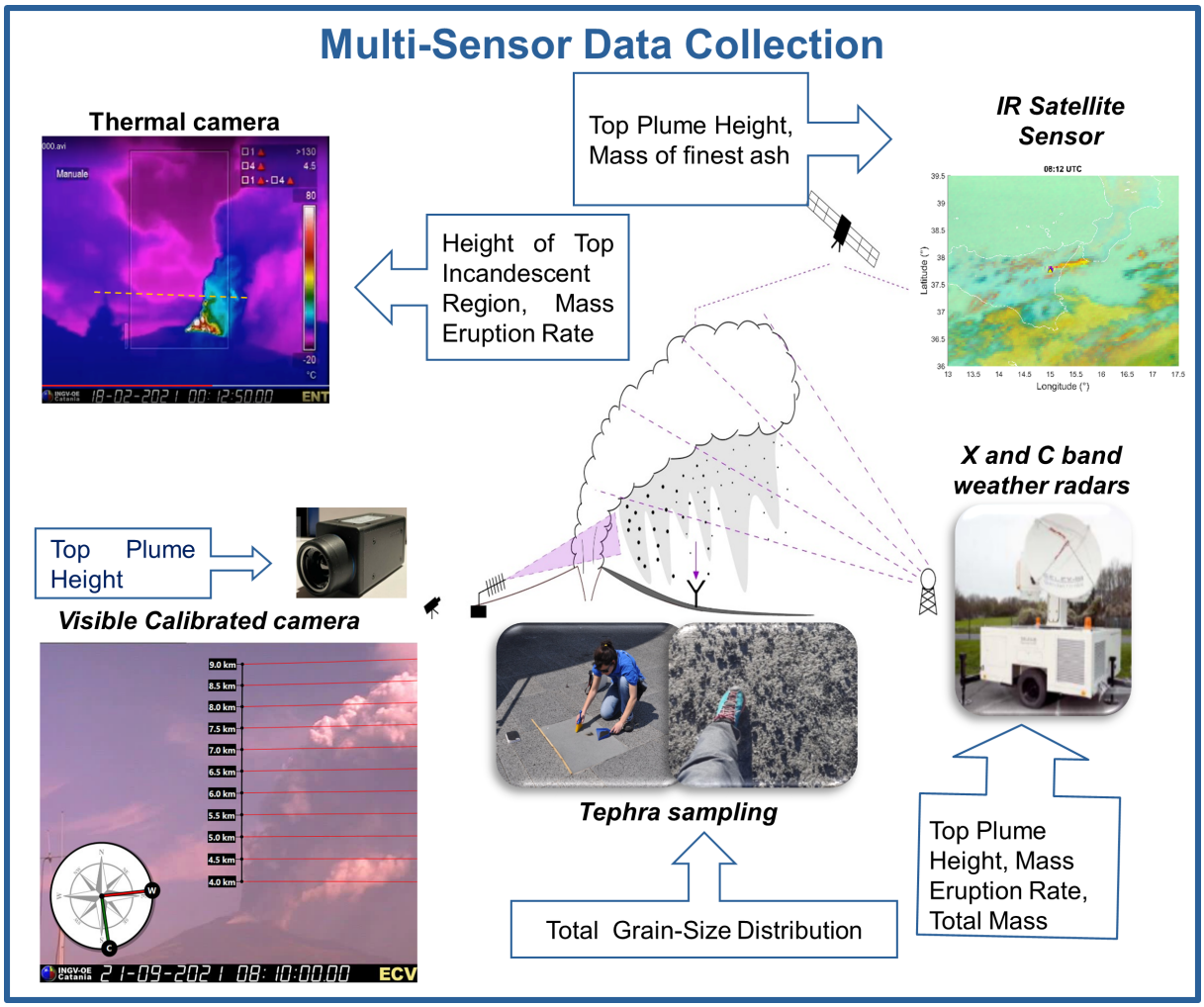

Figure 3. Scheme of the sensors used to retrieve the volcanic plume at Mt. Etna, Italy.

3.2 Modelling

We used the outcomes of two different models used to simulate tephra deposit: TEPHRA2 and Fall3D. The TEPHRA2 model is an updated version of the 2-D advection-diffusion model TEPHRA, based on the advection-diffusion theory (Bonadonna et al., 2005; Connor and Connor, 2006). Additionally, TEPHRA2 employs parallel computing, making it suitable for probabilistic approaches that require numerous, and typically time-consuming, simulations. The main eruption source parameters, required by numerical models, are the column height (CH), the total mass (TM), the grain-size distribution and the density of lithics and juveniles. Other input parameters that need to be calibrated are the diffusion coefficient, which accounts for atmospheric processes including atmospheric diffusion and cloud gravitational spreading, the fall time threshold (FTT) that is an empirical threshold, and the plume ratio that controls the mass distribution within the eruption column. This model is widely used in the monitoring and surveillance system of INGV-OE because it was calibrated using field data of two eruptive scenarios, the 22 July 1998 (Andronico et al., 1999) and the 2002-03 eruptions (Andronico et al., 2008). The main estimated ESP of SPS and WPS (Table 1) were used in the INGV-OE monitoring and forecasting system since 2009 (Scollo et al., 2009). The Fall3D model is a 3-D time-dependent Eulerian scheme based on the advection-diffusion-sedimentation equation (Costa et al., 2006; Folch et al., 2009; Folch et. al., 2021). The model accounts for the turbulent diffusion, given by the gradient transport theory, using as input CH or mass eruption rate, eruption duration and TGSD as eruptive source parameters. In this work, the ECMWF ERA5 reanalysis database (Hersbach et al., 2018, 2020) was used to acquire meteorological data. FALL-3D also integrates several parameterization options for the eruptive column, particle aggregation and domain discretization. The model was widely used to model volcanic ash dispersal and fallout

of Etna eruptions (Poret et al., 2018; Prata et al., 2021; Martinez-Montesinos et al., 2024). Because of its complexity, the model has however a high computational cost, both in terms of time and resources (Costa et al., 2006). For the hazard mapping, we produced hazard curves using the TEPHRA2 and FALL3D models to perform a probabilistic hazard assessment. Probabilistic Volcanic Hazard Assessment (PVHA) represents the most complete scientific contribution for planning rational strategies aimed at managing and mitigating the risks, as it accounts for aleatory and epistemic variability (Tonini et al., 2015). In practice, PVHA requires the exploration of all possible eruptive scenarios to efficiently cover natural variability (Sandri et al., 2016). In these hazard curves, we explored the variability of short and long lasting activities, respectively. For the paroxysms, we explored all the variability in the possible eruptive scenarios as described by the ranges in the ESPs, estimated in Task 2.1, examining the activity for the period 1986-2022. For lateral eruptions, we only considered the 2002-03 eruption because these are the only few events for which quantitative data on the temporal evolution of the MER during the course of the eruption, obtained by the analysis of the deposit (Scollo et al., 2007; Andronico et al., 2008), are available.

4. Results

4.1 Retrieval of eruption source parameters (ESPs) for the model

In this project, several explosive events were analysed to expand the number of eruptive scenarios previously investigated (Scollo et al., 2013). An extensive review of the paroxysmal activity from 1986 to 2022, was conducted using data from literature (239 events) mainly based on work of Andronico et al. (2021) and Calvari and Nunnari (2022). About 50 events have been recently studied in Mereu et al. (2023) that also included a data repository (https://oedatarep.ct.ingv.it/records/975xx-adv58) and in Mereu et al. (2025). Figure 4 shows an example of the combined use of those instruments for the eruptive activity of 21 September 2021 that produced a weak and bent plume (Scollo et al., 2024). For this event, we estimate at approximately 08:10 UTC, a CH value of about 10.9 ± 0.25 km a.s.l. by the radar (Fig. 4a), of about 10.1 ± 1 km a.s.l. by the satellite (Fig. 4b), at a distance of about 70 km from the craters, and of about 8.7 ± 0.5 km by the visible-camera (Fig. 4c).

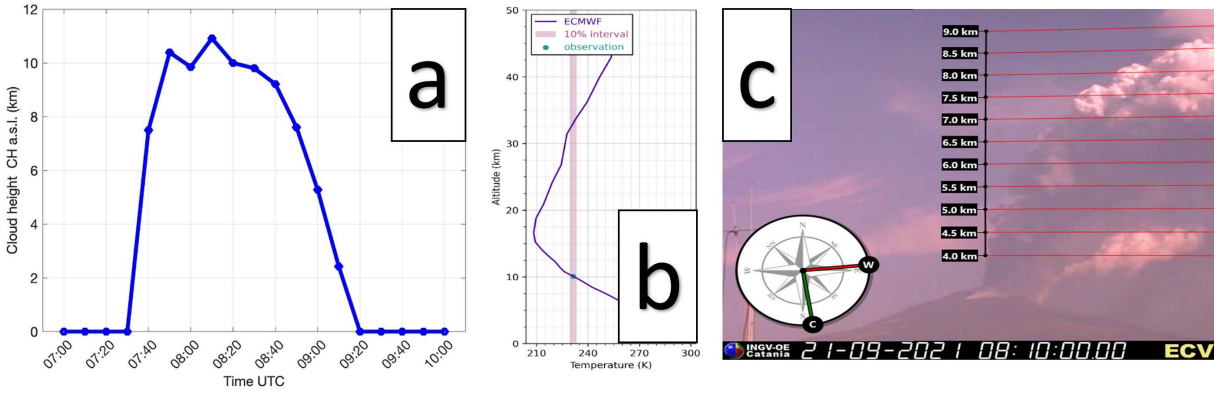

Figure 4. (a) Variation of the column height with time estimated by radar; estimation of the column height at about 08:10 UTC: (b) by satellite; (c) by visible calibrated camera.

Figure 5a shows the MER obtained using three different methods: the red curve using a model based on the buoyant plume theory and assuming a mean wind velocity along the vertical section of volcanic plume (e.g. Degruyter and Bonadonna, 2013), M-DB; the black curve (M-Radar) using the simplified mass continuity approach described in the VARR (Mereu et al., 2015, 2022) methodology; the cyan curve using the divergence theory applied to thermal camera frames (M-TIC) (Mereu et al., 2020, 2022). The cumulative curve shows the TM (Fig. 5b) obtained by integrating by time the three different MERs. Note that we estimated the MER of particles that feed the eruption column and not the total pyroclastic MER that could include all the particles that build the pyroclastic cone. The mean TM is 1.4×10^9 kg, in full agreement with the values erupted during lava fountains at Etna (Scollo et al., 2009). From

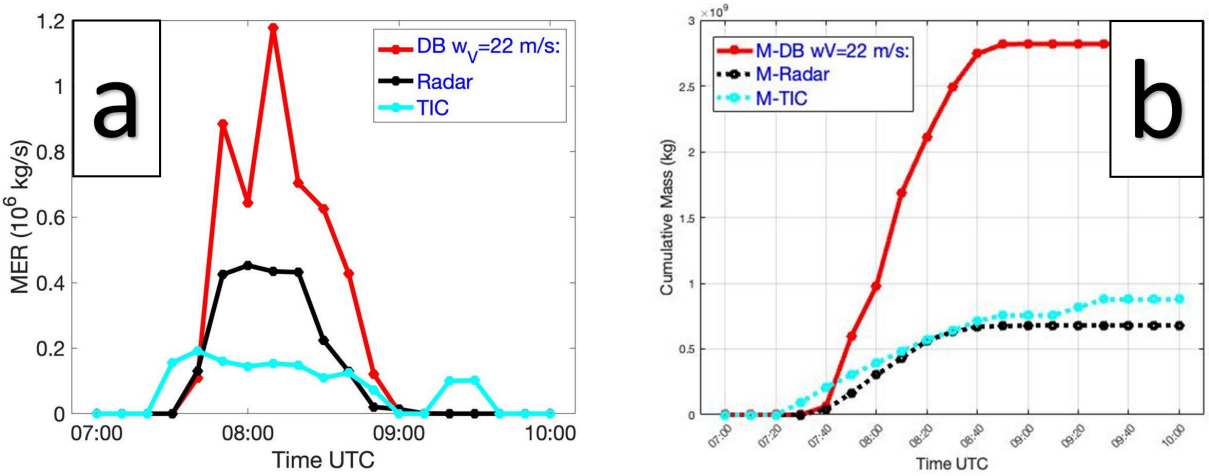

Figure 5. (a) (b) Application of multi sensor data approach for the Etna eruptive event of 21 September 2021.

satellite observations, the estimated total mass of the finest particles is $1.24 \times 10^7 \pm 0.46 \times 10^7$ kg (21:40 UTC), about 1% of TM. The M-DB method shows the largest MER retrievals because it is particularly sensitive to the top plume height estimates, which can be influenced by the crosswind variability and by the consequent plume bending. The M-TIC presents lower results with respect to other methods although consistent in terms of order of magnitude with the M-Radar estimates, but significantly dependent on the estimate of the tephra exit velocity (Mereu et al., 2022). These results are also confirmed by the cumulative mass estimates, as drawn in Fig. 5b.

4.2 Modelling and simulations

In this project, we used both TEPHRA2 and FALL3D models to simulate tephra dispersal in the atmosphere. In particular, for TEPHRA, we further enhanced the simulator's performance by reducing run times and saving the output files in a hierarchical and standard structure, the NetCDF format. This new version also enables the automatic creation of a textual report of the output, along with graphical representations. The TEPHRA2 model was tested and calibrated using data from the deposit of some recent lava fountains (Mereu et al., 2025). Figure 6a shows the results of the daily SPS simulations run at the INGV-OE surveillance system on 21st September 2021 (Scollo et al., 2024).

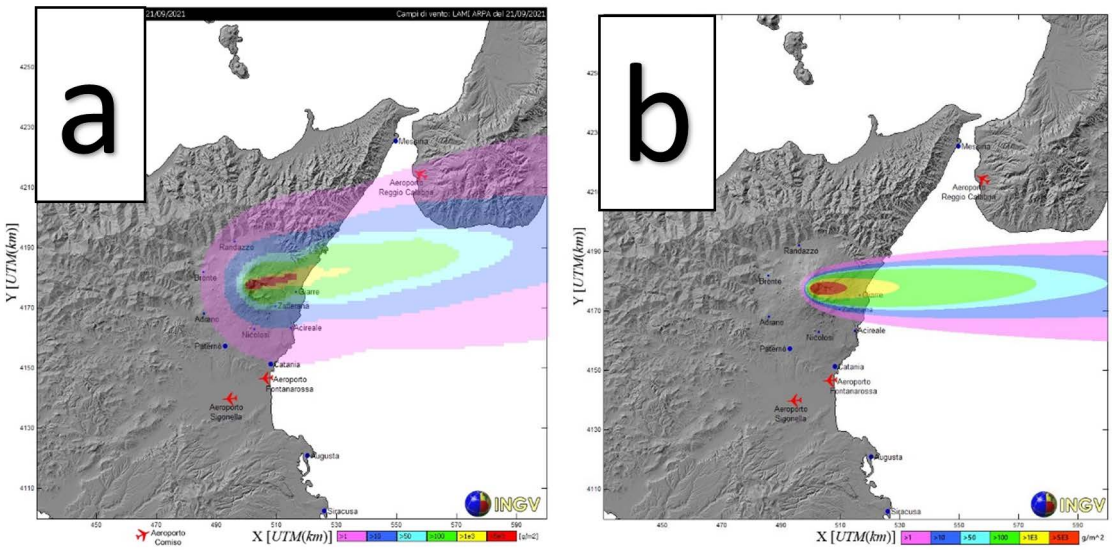

Figure 6. Simulations of Strong Plume Scenario (SPS) (a) versus simulations using input parameters obtained by remote sensing data of the 21 September 2021 (b).

Figure 6b shows the simulations using CH and TM obtained from the remote sensing systems mentioned earlier. Using ESP obtained by remote sensing observations, the volcanic plume has a clear eastern direction and does not reach the Airport of Reggio Calabria. Moreover, the tephra deposit involves a smaller area. During crises, only a qualitative evolution of the main area covered by the fallout is requested and, despite the differences, both simulations require a similar management of the volcanic crisis for civil protection authorities.

Both TEPHRA2 and FALL3D models were applied to estimate the tephra mass deposited on the main road network on the east-southeast flanks of Etna, during the lava fountains of 2021 (Mereu et al., 2025). The use of two numerical models allows for the assessment of the epistemic uncertainty. We produced georeferenced estimates of tephra load deposited on three different municipalities, (Milo, Santa Venerina and Zafferana), which were heavily impacted by the tephra fallout. The ESPs were derived from the analysis of remote sensing data using the methods previously described. Hundreds of simulations were conducted, leading to the production of tephra fallout maps. Figure 7a and 7b show the results of two simulations from the TEPHRA2 and FALL3D models, respectively, for the eruptive activity on 12 June 2021. Figure 7c shows the QGIS displaying the tephra load on the roads (Mere et al., 2025).

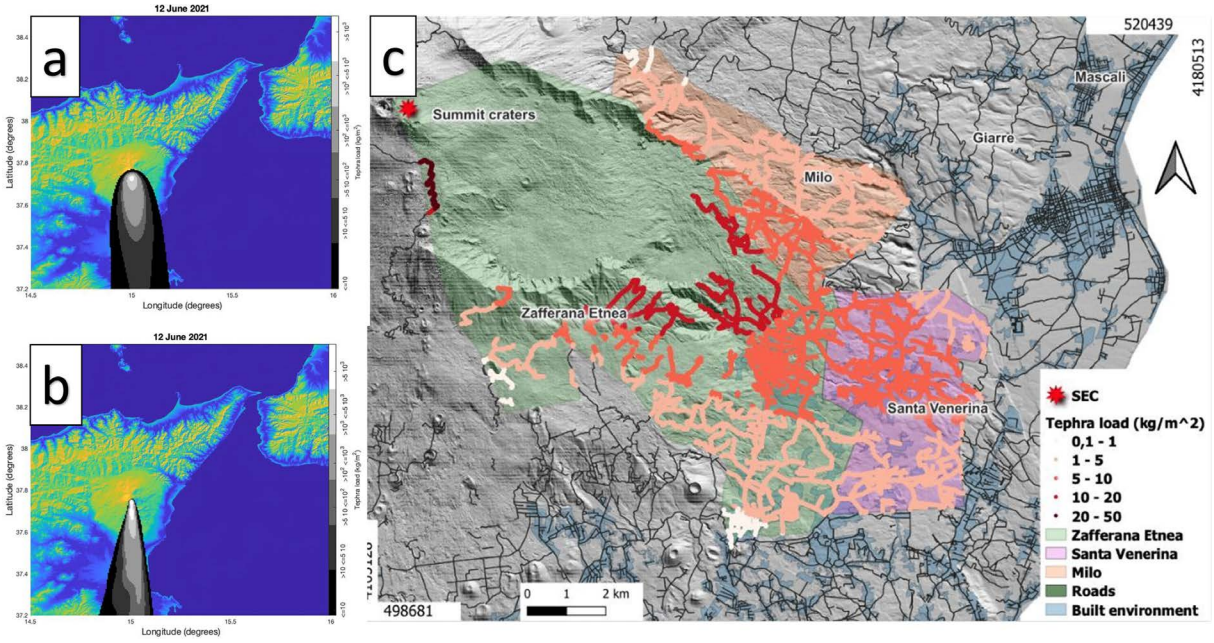

Figure 7. Simulations of 12 June 2021 using the (a) TEPHRA2 and (b) FALL3D mode. (c) Tephra load (kg/m^2) for the Etna explosive event on 28 February 2021, using the TEPHRA2 model. Tephra load is shown in red scale coloured in function of the tephra thresholds on the road network of Milo, Santa Venerina and Zafferana Etnea municipalities, from the paper of Mereu et al. (2025).

4.3 Hazard mapping

A methodological scheme for the hazard mapping is presented in Fig. 8a. Hundreds of TEPHRA2 simulations, where wind variability was also explored, were carried out and results were analysed to produce long-term PVHA through the BET_VH model (Marzocchi et al., 2010), where the epistemic uncertainty is treated through Bayesian inference and the result is a set of hazard curves at each grid point describing the best evaluation hazard, and its uncertainty. To evaluate tephra probabilistic hazard from the paroxysmal activity, we first modelled the temporal occurrence of those events into clusters. We then used the cluster model to build synthetic catalogues of paroxysmal activity. To each synthetic paroxysm, we associated a set of ESP values that were sampled from the empirical distributions built in Task 2.1, and a wind profile corresponding to the one contained in the dataset for that synthetic date. We then simulated the expected tephra deposit with TEPHRA2 on a 500 m × 500 m grid covering the domain shown in Fig. 8b. For lateral eruptions, we first modeled their temporal occurrence. For the summit eruptions, the expected ground load at a given point was aggregated over 1, 3 and 5 years of exposure time, whereas

for flank eruptions, the exposure times considered were 10, 30 and 50 years in agreement with the other hazards in the project (lava flows and seismic events). Results were presented in Sandri et al. (2023) and their analysis is still in progress with a dedicated paper on the realisation of hazard maps for Etna lava fountains. For lateral eruptions we downgraded the spatial grid covered in Sandri et al. (2024) to assess the spatial probability of lateral vent opening at Etna, originally at 200 m × 200 m, to 600 m × 600 m (in total we ended up with 3220 grid cells), to have a computationally lighter problem. Then, we run simulations for each lateral vent position using the TEPHRA2 model, again on the same 500 m grid as above (Fig. 8b). Each simulation was as long as the reference flank eruption occurred in 2002-2003, and its daily MER was computed from the daily column height observed during that eruption (reported, Andronico et al., 2008). For the wind, we used the INGV-OE daily weather data (Scollo et al., 2009) in the period 2007-2019. Each simulation used the reanalysis wind field for a random sampled period from the dataset, covering a period of 65 days as in the 2002-2003 event. Each simulation was then weighted according to the spatial probability of lateral vent opening in its specific spatial cell, and with the temporal probability of lateral eruption. The results of TEPHRA2 simulations, separately for summit and lateral eruptions, were processed to obtain hazard curves on the 500 m grid covering eastern Sicily to Calabria (Fig. 8b). The exceedance probability of tephra accumulation at the ground over selected time windows, and for different load thresholds, were computed, considering a lateral eruption with the main features of 2002-03 Etna eruption and considering the uncertainty on the wind and on the spatial location of the lateral vent or fissure. Figure 8c shows, as an example, the exceedance probability of 5 cm of ground tephra load from a lateral eruption over an exposure window of 10 years. These exceedance probabilities were converted into annual rates to perform multi hazard analysis presented in this issue (Garcia et al., 2025) in an illustrative example over the municipality of Milo (whose borders are shown in Fig. 8c).

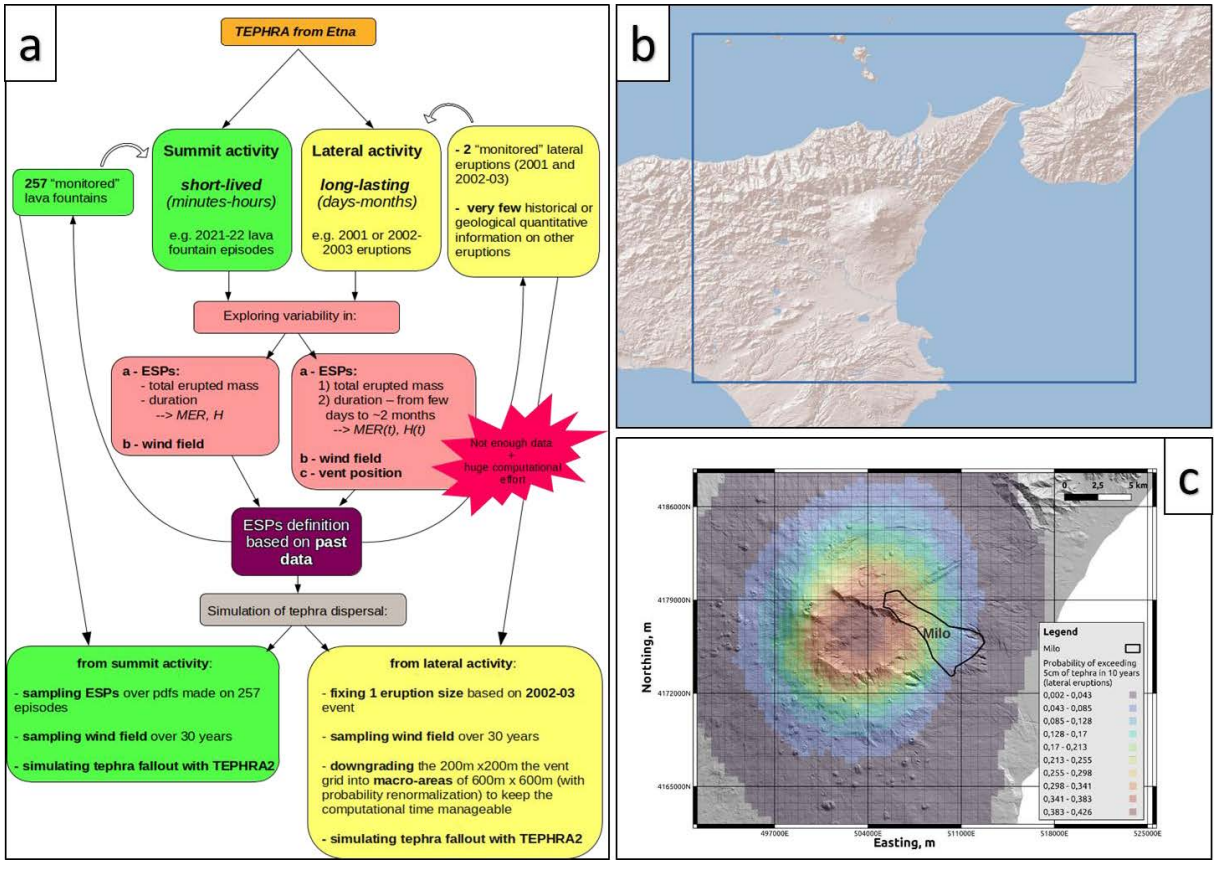

Figure 8. (a) Methodological scheme used to perform hazard mapping; (b) domain covered by the 500 m × 500 m grid used for our simulations covering eastern Sicily to Calabria; (c) exceedance probability of 5 cm of tephra accumulated at the ground in an exposure time window of 10 years, from a lateral eruption with the main features of the 2002-03 Etna eruption, considering wind variability and uncertainty on the vent position (with respect to the computational domain of panel b, here we zoom over the edifice of Etna, and highlight in black solid line the border of the municipality of Milo).

4.4 Other activities

We also briefly describe additional improvements in the retrieval of eruption source parameters and modelling approaches. These activities were carried out also in collaboration with other ongoing projects, further enhancing the accuracy and applicability of our methods.

4.4.1 Improvement in the column height estimation

During the PANACEA project, we began designing a database of calibrated visible images, captured by the INGV-OE cameras. The new database, named CIELO, is currently under development and covers the period between 2014 and 2022. The images were selected based on the VONA messages sent by INGV-OE, and include all instances where the volcanic plume of Etna was visible. Each image was analysed to estimate the time-variation of the column height for each explosive event and then incorporated into the database. In the future, the CIELO database could be used to: (i) improve the understanding of explosive activities at Etna; (ii) validate new techniques for estimating eruptive column heights; (iii) enhance eruption column modelling; (iv) achieve more precise estimates of the mass eruption rate.

Figure 9. Example of images that will be included into the database (under development).

4.4.2 A new relationship between Mass Eruption Rate and Column Height estimated by radar

We analysed radar data from several Etna lava fountains between 2011 and 2021, identifying new radar-based statistical relationships between the MER and the CH. These findings were published in Mereu et al. (2023). According to this study, this relationship is:

$$H_{TP}(MER, v_w) = \alpha e^{\beta \cdot v_w} MER^{\gamma}$$

where v_w represents the mean wind velocity between the Etna's summit craters and CH. For Etna, the values of the α, β, and γ coefficients were derived by analysing 31 lava fountains with median values reported in Mereu et al. (2023). This relationship can be easily applied to radar observations to quickly infer the MER by knowing the CH and v_w. The method also allows for the estimation of the 16th and 84th percentile of the total mass which can be used to assess the uncertainty in the tephra fallout (see details in Mereu et al., 2023). Figure 10 shows three simulations of the tephra deposit from the eruptive activity that occurred on 4 March 2021, lasting one hour with a constant hypothetical height of 11 km a.s.l. We use the 16th, the 50th, and 84th percentile, to define an uncertainty range of the estimated total mass.

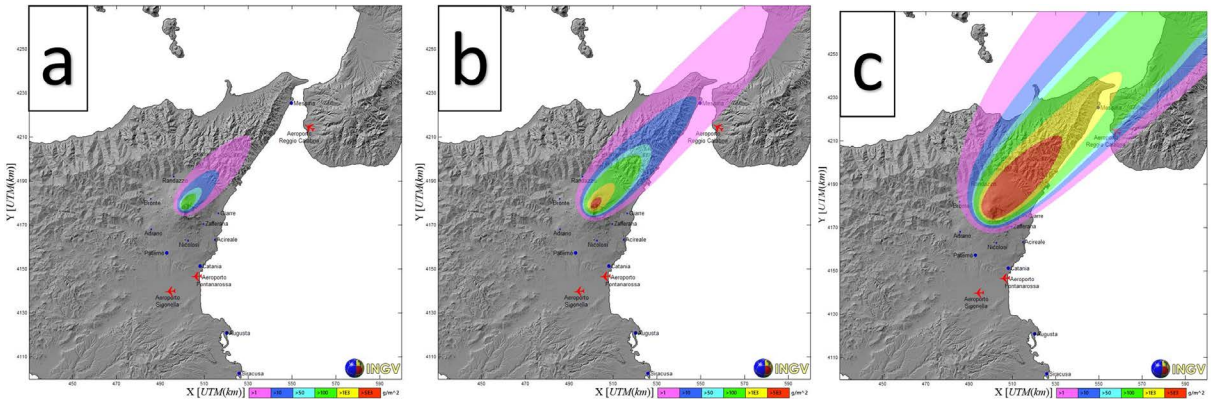

Figure 10. Application of the method proposed in Mereu et al. (2023) for a hypothetical eruption occurred on 4 March 2021 having a column height of 11 km. The results of the simulations were obtained considering the (a) 16th, (b) 50th and (c) 84th percentile of the total mass.

4.4.3 Ballistic Impact

We also investigate the fallout of ballistics during Etna's lava fountains. The aim is to develop a methodology for estimating the area affected by the ballistic fallout in near real-time. For this, we tested and used a well-known ballistic model named Eject! (Mastin, 2001). This trajectory calculator for ballistic clasts is freely available online (https://theghub.org/resources/4543) and estimate the trajectory of bombs/blocks, the maximum distance reached by the clast from the point of emission, the final fallout velocity, and the travel time (Mastin et al., 2001). The model requires several input parameters, including the initial clast ejection velocity (m/s), the ejection angle (degrees from horizontal), the vertical distance between the takeoff point and the landing point (m), the characteristics of the particle (density in kg/m^3 and diameter in cm), the air drag coefficient, the atmospheric properties and the elevation of takeoff point (m a.s.l.). Following the approach described in Costa et al. (2023), and recently applied in Reale Calafino et al. (2025), we assume that, during paroxysms, bombs can fall also within a path starting from the volcanic vent up to the maximum height of the incandescent jet region (IJR) described in Mereu et al. (2020). This assumption increases the elevation of the ballistic takeoff point, reaching greater distance from the vent. We estimate the initial ejection velocity from the IJR height using Bernoulli's law. Additionally, we include the main particle features (e.g. equivalent diameter) measured on the field (e.g. Reale Calafino et al., 2025). Figure 11 shows the Eject! results applied for hypothetical events having features similar to the paroxysm of 23 February 2021.

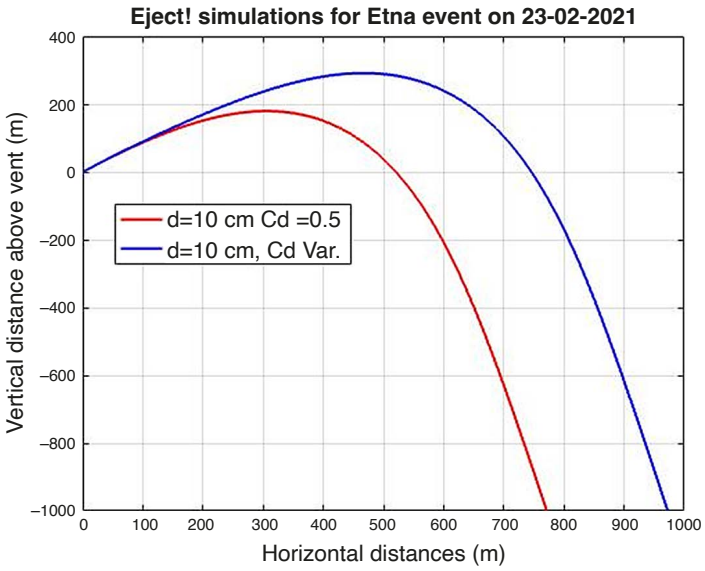

Figure 11. Application of the Eject! model using the proposed method in Costa et al. (2023), considering a bomb of 10 cm.

For the particle, we use a density of 600 kg/m^3 as measured by Reale Calafino et al. (2025), and a hypothetical size of 10 cm. Lastly, we assume an initial velocity of 150 m/s, an ejection angle of 45 degrees and a distance of landing point below take off point 1000 mm, and two different drag coefficients.

5. Discussions

In this work, we present a review of the main activities carried out during the PANACEA project, which aimed at improving the estimation of the hazard from tephra fallout at Mt. Etna, in Italy. We focus specifically on the retrieval of ESPs using various remote sensing systems and applying different models to enhance the tephra fallout hazard mapping. Etna is highly active, and during paroxysms, it generates high eruption columns and significant tephra fallout that blankets the volcano's flanks, causing various issues. For instance, such events often lead to the closure of airspace around Catania airport, with several flights being diverted to nearby airports, such as Palermo and Comiso. The abundant tephra fallout also damages infrastructure, and after these episodes, local authorities frequently impose traffic restrictions. Speed limits are often reduced to 30 km/h, and the circulation of two-wheeled vehicles, including bicycles, is prohibited to prevent accidents caused by ash-covered streets. Additionally, extensive damages to crops, particularly on the eastern and southeastern slopes of Etna, are common, mainly for the prevailing winds (Barsotti et al., 2010; Scollo et al., 2013). Fruits, for example, can be severely affected by tephra fallout, either due to the impact of lapilli or abrasions to the peel. Given these impacts, improvements in the tephra hazard assessments, as also developed in this paper, are an important measure to mitigate the effects of the volcanic activity.

Remote sensing data plays a critical role in the real-time characterization of volcanic plumes and clouds (Mota et al., 2024). These data sources range from ground-based sensors (e.g., lidar, cameras, radar) to satellite-based approaches, which are widely utilized due to their accessibility and comprehensive coverage (Mota et al., 2024). When processed in near-real time, these data provide valuable support to volcanologists, helping to constrain ESPs (Engwell et al., 2024) and identify eruptive scenarios, such as the WPS versus the SPS (Scollo et al., 2019). For example, at Etna, visible calibrated images and satellite data are used to estimate the column heights. This information is included in the VONA messages, which are sent to aviation authorities, including the VAACs.

In general, it is crucial to understand how different remote sensing techniques can be synergically combined for a more comprehensive volcanic monitoring. Different sensors are suited to monitor different regions of the volcanic plume and clouds. For example, visible calibrated cameras at Etna capture only the column height above the vent whereas satellites can estimate the plume height even several kilometers away from the vent. However, since various sensors are sensitive to different particle sizes, comparing their estimates is not always straightforward. Some methods can be only made under precise conditions; for example, the darkest pixel method requires the

volcanic plume to be optically thick (Scollo et al., 2019). For these reasons, we agree with Mota et al. (2024), on the importance of employing multiplatform approaches when data are available. This strategy helps to overcome the inherent limitations of individual remote sensing techniques, providing more robust and reliable observations. Despite these limits, we emphasise that the use of remote sensing systems significantly enhances our ability to improve the tephra fallout hazard assessment. In volcano observatories, daily simulations are performed using a limited number of scenarios (Engwell et al., 2024). During volcanic crises, data from remote sensing systems can greatly assist the volcanologists in identifying the most appropriate scenarios. At Etna Volcano Observatory those data help to distinguishing between WPS and SPS and the results of the simulations are reported in the reports provided to the Italian Civil Protection and available to the volcanologist on duty (https://www.ct.ingv.it/index.php/monitoraggio-e-sorveglianza/prodotti-del-monitoraggio/comunicati-attivita-vulcanica). Moreover, data from remote sensing systems can expand the already existing dataset of ESP (Aubry et al., 2021), enabling more reliable hazard mapping (Sandri et al., 2023). Data from remote sensing systems can substantially improve these simulations by providing more accurate constraints on the results. However, reducing uncertainty in the ESP estimations remains a critical challenge. For instance, Fig. 10 shows that the uncertainty in the total mass is still considerable. We believe future efforts should focus on improving the retrieval techniques from remote sensing systems. This can be achieved through a continuous comparison between model results and field data, enabling advancements in our understanding of physical processes that govern eruption columns, volcanic plume and cloud dispersal and tephra fallout. To this end, we plan to conduct new comparisons among the computed results, using ESP obtained from remote sensing, and field data collected during the most recent volcanic crises at Etna. Currently, simulations of WPS or SPS are used by the on-duty volcanologists to quickly identify the most likely areas affected by fallout, without quantifying the tephra load deposited on the ground, that is quantified later by field campaigns. Perhaps in future, data assimilation techniques (Mingari et al., 2022) could be used to give more reliable tephra deposit loads, including that information in the communication to the authorities.

Finally, updating new procedures is still needed. For example, although large clast and ballistic simulations have recently been tested, they have not yet been incorporated into communications. We hope that, in the future, these components will be integrated into operations, along with robust uncertainty estimates for both modeling and observational data.

Data availability statement. Images and analysis can be requested of the author.

Acknowledgements. The work was funded by the INGV-MIUR project Pianeta Dinamico "Working Earth" PANACEA project and partially by the Sub-projects VT-DYNAMO-2023, by the Sub-project SAFARI-2023 and by the Space It Up project. We thank technicians and technologists who take care of the INGV-OE camera network, the volcanologists of INGV-OE who regularly collect data during volcanic events. This work was also funded by the Italian Presidenza del Consiglio dei Ministri – Dipartimento della Protezione Civile (DPC). This paper does not necessarily represent DPC official opinion and policies.

References

Alparone, S., D. Andronico, L. Lodato and T. Sgroi (2003). Relationship between tremor and volcanic activity during the Southeast Crater eruption on Mount Etna in early 2000, J. Geophys. Res., 108, B5, 2241, doi:10.1029/2002JB001866.

Andronico, D., P. Del Carlo and M. Coltelli (1999). The 22 July 1998 fire fountain episode at Voragine Crater (Mt Etna, Italy), Volcanic and Magmatic Studies Group (VMSG), Annual Meeting, Birmingham, 5-6 January.

Andronico, D., S. Scollo, A. Cristaldi and S. Caruso (2008). The 2002-03 Etna explosive activity: Tephra dispersal and features of the deposit, J. Geophys. Res., 113, B04209, doi:10.1029/2007JB005126.

Andronico, D., A. Cannata, G. Di Grazia and F. Ferrari, (2021). The 1986-2021 paroxysmal episodes at the summit craters of Mt. Etna: Insights into volcano dynamics and hazard, Earth Sci. Rev., 220, 103686, doi:10.1016/j.earscirev.2021.103686.

Aubry, T. J., S. Engwell, C. Bonadonna, G. Carazzo et al. (2021). The Independent Volcanic Eruption Source Parameter Archive (IVESPA, version 1.0): a new observational database to support explosive eruptive column model validation and development, J. Volcanol. Geotherm. Res., 417, 107295, doi:10.1016/j.jvolgeores.2021.107295.

Barsotti, S., C. D'Oriano, A. Neri, R. Cioni et al. (2013). Tephra-fallout hazard of Violent Strombolian eruptions at Vesuvius: insights from the 1906 event, EGU General Assembly Conference Abstracts, EGU2013-10481, European Geosciences Union, Vienna.

Barsotti, S., S. Scollo, G. Macedonio, A. Felpeto et al. (2024). The European Volcano Observatories and their use of the aviation colour code system, Bull. Volcanol., 86, 3, 23, doi:10.1007/s00445-024-01712-0.

Barsotti, S., D. Andronico, A. Neri, P. Del Carlo et al. (2010). Quantitative assessment of volcanic ash hazards for health and infrastructure at Mt. Etna (Italy) by numerical simulation, J. Volcanol. Geotherm. Res., 192, 85-96, doi:10.1016/j.jvolgeores.2010.02.011.

Behncke, B., S. Branca, R. A. Corsaro, E. De Beni et al. (2014). The 2011-2012 summit activity of Mount Etna: Birth, growth and products of the new SE crater, J. Volcanol. Geotherm. Res., 270, 10-21, doi:10.1016/j.jvolgeores.2013.11.012.

Bonaccorso, A. and S. Calvari (2013). Major effusive eruptions and recent lava fountains: Balance between expected and erupted magma volumes at Etna volcano, Geophys. Res. Lett., 40, 6069-6073, doi:10.1002/2013GL058291.

Bonaccorso, A., S. Calvari, A. Linde and S. Sacks (2014). Eruptive processes leading to the most explosive lava fountain at Etna volcano: The 23 November 2013 episode, Geophys. Res. Lett., 41, 14, 4912-4919, doi:10.1002/2014GL060623.

Bonadonna, C., C. B. Connor, B. F. Houghton, L. Connor et al. (2005). Probabilistic modeling of tephra dispersal: Hazard assessment of a multiphase rhyolitic eruption at Tarawera, New Zealand, J. Geophys. Res., 110, B03203, doi:10.1029/2003JB002896.

Branca, S. and P. Del Carlo (2005) Types of eruptions of Etna volcano AD 1670-2003: implications for short-term eruptive behaviour, Bull. Volcanol., 67, 8, 732-742, doi:10.1007/s00445-005-0412-z.

Calvari, S. and G. Nunnari (2022). Etna Output Rate during the Last Decade (2011-2022): Insights for Hazard Assessment, Remote Sens., 14, 23, 6183, doi:10.3390/rs14236183.

Calvari, S., F. Cannavò, A. Bonaccorso, L. Spampinato et al. (2018). Paroxysmal Explosions, Lava Fountains and Ash Plumes at Etna Volcano: Eruptive Processes and Hazard Implications, Front. Earth Sci., 6, 107, doi:10.3389/feart.2018.00107.

Calvari, S., G. Bilotta, A. Bonaccorso, T. Caltabiano et al. (2019). The VEI 2 Christmas 2018 Etna eruption: A small but intense eruptive event or the starting phase of a larger one?, Remote Sens., 12, 905, doi:10.3390/rs12060905.

Calvari, S., G. G. Salerno, L. Spampinato, M. Gouhier et al. (2011). An unloading foam model to constrain Etna's 11-13 January 2011 lava fountaining episode, J. Geophys. Res., 116, B11207, doi:10.1029/2011JB008297.

Connor, L. G. and C. B. Connor (2006). Inversion is the key to dispersion: Understanding eruption dynamics by inverting tephra fallout, Statistics in Volcanology, Mader, H. M., Geol. Soc. London, 231-242.

Costa, A., G. Macedonio and A. Folch (2006). A three-dimensional Eulerian model for transport and deposition of volcanic ashes, Earth Planet. Sci. Lett., 241, 3-4, 634-647, doi:10.1016/j.epsl.2005.11.019.

Costa, G., L. Mereu, M. Prestifilippo, S. Scollo et al. (2023). Modeling the Trajectories of Ballistics in the Summit Area of Mt. Etna (Italy) during the 2020-2022 Sequence of Lava Fountains, Geosciences, 13, 5, 145, doi:10.3390/geosciences13050145.

Degruyter, W. and C. Bonadonna (2013). Improving on mass flow rate estimates of volcanic eruptions, Geophys. Res. Lett., 39, 16, 16308, doi:10.1029/2012GL052566.

Engwell, S., L. G., Mastin, C. Bonadonna, S. Barsotti et al. (2024). Characterising, quantifying, and accessing eruption source parameters of explosive volcanic eruptions for operational simulation of tephra dispersion: a current view and future perspectives, Bull Volcanol, 86, 67, doi:10.1007/s00445-024-01706-y.

Folch, A., A. Costa and G. Macedonio (2009). FALL3D: A computational model for transport and deposition of volcanic ash, Comput. Geosci., 35, 6, 1334-1342, doi:10.1016/j.cageo.2008.08.008.

Folch, A., L. Mingari, N. Gutierrez, M. Hanzich et al. (2020). FALL3D-8.0: a computational model for atmospheric transport and deposition of particles, aerosols and radionuclides – Part 1: Model physics and numerics, Geosci. Model Dev., 13, 1431-1458, doi:10.5194/gmd-13-1431-2020.

Garcia, A., L. Sandri, V. Pessina, F. Meroni et al. (2025). A target-based, multi-hazard assessment approach as a tool for supporting decision-making in volcanic areas: a case study in Mt. Etna, Italy, Ann. Geophys., 68, 1, doi:10.4401/ag-9173.

Guffanti, M., J. W. Ewert, G. M. Gallina, G. J. S. Bluth et al. (2005). Volcanic-ash hazard to aviation during the 2003-2004 eruptive activity of Anatahan volcano, Commonwealth of the Northern Mariana Islands, J. Volcanol. Geotherm. Res., 146, 241-255, doi:10.1016/j.jvolgeores.2004.12.011.

Hersbach, H., B. Bell, B. Berrisford, P. Biavati et al. (2018). ERA5 hourly data on pressure levels from 1959 to present, ERA5 Data, 1999-2049, doi:10.24381/cds.bd0915c6.

Hersbach, H., B. Bell, P. Berrisford, S. Hirahara et al. (2020). The ERA5 global reanalysis, Q. J. Roy. Meteor. Soc., 146,730, 1999-2049, doi:10.1002/qj.3803.

Hayes, J. L., T. M. Wilson, C. Brown, N. I. Deligne et al. (2021). Assessing urban disaster waste management requirements after volcanic eruptions, Int. J. Disaster Risk Reduct., 52, 6, 101935, doi:10.1016/j.ijdrr.2020.101935.

Jenkins, S. F., A. McSporran, T. M. Wilson, C. Stewart et al. (2024). Tephra fall impacts to buildings: the 2017-2018 Manaro Voui eruption, Vanuatu. Front. Earth Sci., 12, 1392098, doi:10.3389/feart.2024.1392098.

Horwell, C. J. and P. Baxter (2006). The respiratory health hazards of volcanic ash: a review for volcanic risk mitigation, Bull.Volcanol., 69, 1-24, doi:10.1007/s00445-006-0052-y.

Lechner, P., A. G. Tupper, M. Guffanti, S. Loughlin et al. (2017). Volcanic ash and aviation-the challenges of real-time, global communication of a natural hazard, Springer, 51-64, doi:10.1007/11157_2016_49.

Martínez Montesinos, B., L. Mingari, E. Caruso, M. Poret et al. (2024). Application of data assimilation to reconstruct the 3-5 December 2015 Etna eruption, ESS Open Arch., doi:10.22541/essoar.172616137.73255926/v1.

Marzano, F. S., E. Picciotti, G. F. Vulpiani and M. Montopoli (2012). Synthetic signatures of volcanic ash cloud particles from X-band dual-polarization radar, IEEE Trans. Geosci. Remote Sens., 50, 1, 193-211, doi:10.1109/TGRS.2011.2159225.

Mastin, L. G. (2001). Insights into volcanic conduit flow from an open-source numerical model, Geochem., Geophys., Geosyst., 3, 7, 1-18, doi:10.1029/2001GC000192.

Mereu, L., F. S. Marzano, M. Montopoli and C. Bonadonna (2015). Retrieval of tephra size spectra and mass flow rate from C-band radar during the 2010 Eyjafjallajökull eruption, Iceland, IEEE Trans. Geosci. Remote Sens., 53, 10, 5644-5660, doi:10.1109/tgrs.2015.2427032.

Mereu, L., S. Scollo, C. Bonadonna, V. Freret Lorgeril et al. (2020). Multisensor characterization of the incandescent jet region of lava fountain-fed tephra plumes, Remote Sens., 12, 21, 3629, doi:10.3390/rs12213629.

Mereu, L., S. Scollo, C. Bonadonna, F. Donnadieu et al. (2022). Ground-based remote sensing of volcanic mass flow: Retrieval techniques and uncertainty analysis of Mt. Etna eruptions in 2015. IEEE J. Sel. Top. Appl. Earth Obs. Remote Sens., 15, 504-518, doi:10.1109/jstars.2021.3133946.

Mereu, L., S. Scollo, A. Garcia, L. Sandri et al. (2023). A new radar-based statistical model to quantify mass eruption rate of volcanic plumes, Geophys. Res. Lett., 50, 7, e2022GL100596, doi:10.1029/2022GL100596.

Mereu, L. and S. Scollo (2024). Detecting Etna Explosive Activity by X- and C-Band Radars, IGARSS 2024-2024 IEEE International Geoscience and Remote Sensing Symposium, Athens, Greece, 2153-7003, doi:10.1109/IGARSS53475.2024.10641519.

Mereu, L., M. Stocchi, A. Garcia, M. Prestifilippo et al. (2025). Estimating the mass of tephra accumulated on roads to best manage the impact of volcanic eruptions: the example of Mt. Etna, Italy, Nat. Hazards Earth Syst. Sci., https://egusphere.copernicus.org/preprints/2024/egusphere-2024-2028/.

Miller, T. P. and T. J. Casadevall (2000). Volcanic ash hazards to aviation, Encyclopedia of Volcanoes, 1, Sigurdsson, H., B. Houghton, H. Rymer, J. Stix, S. McNutt (Eds.), Academic Press, San Diego, CA, USA, 915-930.

Mingari, L., A. Folch, A. T. Prata, F. Pardini et al. (2022). Data assimilation of volcanic aerosol observations using FALL3D+PDAF, Atmos. Chem. Phys., 22, 1773-1792, doi:10.5194/acp-22-1773-2022.

Mota, R., J. M. Pacheco, A. Pimentel and A. Gil (2024). Monitoring volcanic plumes and clouds using remote sensing: A systematic review, Remote Sens., 16, 1789, doi:10.3390/rs16101789.

Neri, M., V. Acocella, B. Behncke, V. Maiolino et al. (2005). Contrasting triggering mechanisms of the 2001 and 2002-2003 eruptions of Mount Etna (Italy), J. Volcanol. Geotherm. Res., 144, 1-4, 235-255, doi:10.1016/j.jvolgeores.2004.11.025.

Newhall, C. G. and S. Self (1982). The volcanic explosivity index (VEI): An estimate of explosive magnitude for historical volcanism, J. Volcanol. Geotherm. Res., 87, 1231-1238, doi:10.1029/JC087iC02p01231.

Osman, S., E. Rossi, C. Bonadonna, C. Frischknecht et al. (2019). Exposure-based risk assessment and emergency management associated with the fallout of large clasts at Mount Etna, Nat. Hazards Earth Syst. Sci., 19, 3, 589-610, doi:10.5194/nhess-19-589-2019.

Pioli, L., E. Erlund, E. Jonhson, K. Cashmann et al. (2008). Explosive dynamics of violent strombolian eruptions: the eruption of parícutin volcano 1943-1952 (Mexico), Earth Planet. Sci. Lett., 271, 359-368, doi:10.1016/j.epsl.2008.04.026.

Poret, M., S. Corradini, L. Merucci, A. Costa et al. (2018). Reconstructing volcanic plume evolution integrating satellite and ground-based data: application to the 23 November 2013 Etna eruption, Atmos. Chem. Phys., 18, 4695-4714, doi:10.5194/acp-18-4695-2018.

Prata, A. T., L. Mingari, A. Folch, G. Macedonio et al. (2021). FALL3D-8.0: a computational model for atmospheric transport and deposition of particles, aerosols and radionuclides – Part 2: Model validation, Geosci. Model Dev., 14, 409-436, doi:10.5194/gmd-14-409-2021.

Reale Calafino, M., L. Mereu, D. Messina, M. Cantarero et al. (2025). 3D reconstruction of volcanic bombs to enhance ballistic trajectory predictions, Ann. Geophys., 68, 1, doi:10.4401/ag-9134.

Romeo, F., L. Mereu, S. Scollo, M. Papa et al. (2023). Volcanic cloud detection and retrieval using satellite multisensor observations, Remote Sens., 15, 4, 888, doi:10.3390/rs15040888.

Rossi, E., C. Bonadonna and W. Degruyter (2019). A new strategy for the estimation of plume height from clast dispersal in various atmospheric and eruptive conditions, Earth Planet. Sci. Lett., 505, 1-12, doi:10.1016/j.epsl.2018.10.007.

Sandri, L., A. Costa, J. Selva, R. Tonini et al. (2016). Beyond eruptive scenarios: assessing tephra fallout hazard from Neapolitan volcanoes, Sci. Rep., 6, 24271, doi:10.1038/srep24271.

Sandri, L., L. Mereu, A. Garcia, M. Prestifilippo et al. (2023). Assessing tephra fall hazard from Etna paroxysms: modelling their temporal occurrence and ash dispersion based on an integrated catalogue from literature data and radar-and satellite-derived data, ID 231, Cities on Volcanoes 12, Antigua, Guatemala, 11-17 February 2024.

Sandri, L., A. Garcia, C. Proietti, S. Branca et al. (2024). Where will the next flank eruption at Etna occur? An updated spatial probabilistic assessment, Nat. Hazards Earth Syst. Sci., 24, 12, 4431-4455, doi:10.5194/nhess-24-4431-2024.

Scollo, S., P. Del Carlo and M. Coltelli (2007). Tephra fallout of 2001 Etna flank eruption: Analysis of the deposit and plume dispersion, J. Volcanol. Geotherm. Res., 160, 1-2, 147-164, doi:10.1016/j.jvolgeores.2006.09.007.

Scollo, S., A. Folch and A. Costa (2008). A parametric and comparative study of different tephra fallout models, J. Volcanol. Geotherm. Res., S. Smith (Editor), Elsevier, Oxford, 176, 2, 199-211, ISSN: 0377-0273, doi:10.1016/j.jvolgeores.2008.04.002.

Scollo, S., M. Prestifilippo, G. Spata, M. D'Agostino et al. (2009). Monitoring and forecasting Etna volcanic plumes, Nat. Hazards Earth Syst. Sci., 9, 5, 1573-1585, doi:10.5194/nhess-9-1573-2009.

Scollo, S., M. Coltelli, C. Bonadonna and P. Del Carlo (2013). Tephra hazard assessment at Mt. Etna (Italy), Nat. Hazards Earth Syst. Sci., 13, 3221-3233, doi:10.5194/nhess-13-3221-2013.

Scollo, S., A. Boselli, M. Coltelli, G. Leto et al. (2014). Combining observations and model simulations to reduce the hazard of Etna volcanic ash plumes, Geophys. Res. Abstr., 16, 1, ISSN 1607-7962.

Scollo, S., M. Prestifilippo, C. Bonadonna, R. Cioni et al. (2019). Near-real-time tephra fallout assessment at Mt. Etna, Italy, Remote Sens., 11, 24, 2987, doi:10.3390/rs11242987.

Scollo, S., L. Mereu, M. Prestifilippo and F. Romeo (2024). Characterization of volcanic plumes by remote sensing sensors: an example from Etna volcano, IGARSS 2024-2024 IEEE International Geoscience and Remote Sensing Symposium, Athens, Greece, 2024, 3817-3820, doi:10.1109/IGARSS53475.2024.10642244.

Sparks, R. S. J., M. I. Bursik, S. N. Carey, J. S. Gilbert et al. (1997). Volcanic Plumes, John Wileys & Sons, Chichester, U.K, 557, ISBN: 0-471-94985-X.

Tonini, R., L. Sandri, A. Costa and J. Selva (2015). Brief Communication: The effect of submerged vents on probabilistic hazard assessment for tephra fallout, Nat. Hazards Earth Syst. Sci., 15, 409-415, doi:10.5194/nhess-15-409-2015.

Viccaro, M., I. Garozzo, A. Cannata, G. Di Grazia et al. (2014). Gas burst vs. gas-rich magma recharge: A multidisciplinary study to reveal factors controlling duration of the recent paroxysmal eruptions at Mt. Etna, J. Volcanol. Geotherm. Res., 278-279, 1-13, doi:10.1016/j.jvolgeores.2014.04.001.

Wilson, T. M., C. Stewart, V. Sword-Daniels, G. S. Leonard et al. (2012). Volcanic ash impacts on critical infrastructure, Phys. Chem. Earth, Parts A/B/C, 45-46, 5-23, doi:10.1016/j.pce.2011.06.006.

Wilson, G., T. M. Wilson, N. I. Deligne, D. M. Blake et al. (2017). Framework for developing volcanic fragility functions for critical infrastructure, J. Appl.Volcanol., 6-14, doi:10.1186/s13617-017-0065-6.

***CORRESPONDING AUTHOR: Simona SCOLLO**,
Istituto Nazionale di Geofisica e Vulcanologia, Osservatorio Etneo, Catania, Itali
e-mail: simona.scollo@ingv.it